Ultrafast laser-induced plasma anisotropy in pristine and surface pre-structured zinc telluride, probed by terahertz pulses

Daiwei Zhang, N Sedao, Nicolas Faure, Yannick Bleu, Razvan Stoian, Ciro D'amico

Research Article | Vol. 31, No. 15 / 17 Jul 2023 / Optics Express 24054
Optics EXPRESS

Ultrafast laser-induced plasma anisotropy in pristine and surface pre-structured zinc telluride, probed by terahertz pulses

DAIWEI ZHANG, N SEDAO, NICOLAS FAURE, YANNICK BLEU, RAZVAN STOIAN, AND CIRO D'AMICO*

Université Jean Monnet Saint-Etienne, CNRS, Institut d'Optique Graduate School, Laboratoire Hubert Curien UMR 5516, F-42023, Saint-Etienne, France
ciro.damico@univ-st-etienne.fr

Abstract: We use THz probe pulses to detect and analyze the dynamics of charge transport anisotropies generated by ultrafast laser two-photon absorption in Zinc Telluride (ZnTe) semi-insulating crystal showing smooth and laser structured surfaces. The detected anisotropy consists in a modulation of the THz transmission as a function of the orientation of the <001> axis of ZnTe. The change in THz transmission after pump excitation is attributed to free carrier absorption of the THz field in the laser-induced electron-hole plasma. Pre-structuring the surface sample with laser-induced periodic surface structures (ripples) has strong influence on free carrier THz transmission and its associated anisotropic oscillation. Within the relaxation dynamics of the laser-induced free carriers, two relaxation times have to be considered in order to correctly describe the dynamics, a fast relaxation, of about 50 picoseconds in pristine sample (90 picoseconds in sample pre-structured with ripples), and a slow one, of about 1.5 nanoseconds. A theoretical model based on classical Drude theory and on the dependence of the two-photon absorption coefficient with the crystal orientation and with the laser polarization is used to fit the experimental results.

1. Introduction

Engineering and functionalization of materials by ultrafast direct laser processing [1], in bulk or on surfaces, is a promising way for the development of integrated and smart photonic devices, for applications in several domains of science [2–4]. Effects of laser-induced ripples structures on material surfaces have been studied during the last decades for several materials. These periodic anisotropic structures are the result of laser scattering and interference, creating periodic patterns with periodicities proportional to the wavelength [5]. They can add to a structured material new characteristic in the optical, thermal, or mechanical domains [5–7]. Being defined by light-driven excitation and ionization processes, the question of potential transport anisotropies is of interest. On the other hand, since the earliest works on ionization process in semiconductors and other crystalline materials much attention has been devoted to the study of the anisotropies involved in these processes, especially when related to two-photon absorption (TPA) in low bandgap semi-insulating crystals [8–13]. If the second-order optical susceptibility is important for the design of electrooptic and frequency doubling devices, the third-order susceptibility related to TPA can give fundamental limitations to any high $\chi^{(3)}$ material in all-optical switching schemes based on an intensity-dependent refractive index [14–16].

The anisotropy of TPA coefficient has been studied in GaAs, CdTe and InSb [17–19], showing that it is a function of the crystal orientation and of the polarization direction of the incident light. Sanjuan et *al*. [20] studied the influence of TPA anisotropy on THz generation by Optical Rectification (OR) in a <111> cut ZnTe crystal.

#491596 https://doi.org/10.1364/OE.491596
Journal © 2023 Received 24 Mar 2023; revised 19 May 2023; accepted 29 May 2023; published 7 Jul 2023

Optics EXPRESS

Concerning the recombination process after TPA excitation of semi-conducting crystals, Kanevce et *al*. [21] studied carrier dynamics and transport characteristics within two-photon excited photoluminescence in CdTe semiconductor. Opanowicz et *al*. [22] discussed the luminescence of highly excited ZnTe crystals under several experimental conditions showing that the recombination rate of free carriers can be described in terms of direct band-to-band transition and direct electron-hole (e-h) trapping. Baxter et *al*. [23] proved that electrons and holes have similar effective masses upon excitation from the valence band to the conduction band via TPA and both will contribute to the THz absorption in bulk ZnO by time-resolved terahertz spectroscopy.

However, so far, little experimental works have been devoted to the study of the relaxation dynamics by considering the anisotropic aspect of ultrafast TPA excitation of low band-gap crystals and, to our knowledge, no works can be found in the literature concerning laser pre-structured samples with topography anisotropies. In this work we will investigate the anisotropic dynamics which follows the initial TPA excitation, in pristine and surface pre-structured samples. Among the methods which can be proposed for the study of crystalline and electronic band asymmetries in semi-insulating crystals [17,24], here we use optical pump and terahertz probe pulses, which is a very powerful method for non-invasive in situ analysis of free carrier conductivity. Moreover, using THz pulses as a probe has the advantage of high free carrier absorption in the laser-induced plasma, the absorption cross-section at THz frequencies being about 10^8 times larger than at optical frequencies (800 nm in the present case). This means that electron densities as low as 10^{13} – $10^{14} cm^{-3}$ can be detected and their relaxation dynamics analyzed in a context of low-density electron-hole plasmas and relatively long collision times. The anisotropy of TPA gives an initial modulation of the THz response of ZnTe crystal as a function of the crystal orientation. This will induce THz transmission oscillations, by which conductivity changes of the excited ZnTe can eventually be deduced. We will show that the model of TPA anisotropy given in Ref. [17] can be applied in our case, fitting in a satisfactory way the experimental results. By adjusting the theoretical model to our experimental data, we are able to deduce some important parameters related to TPA anisotropy and the relaxation dynamics in ZnTe after ultrafast laser excitation, in presence and in absence of surface ripples.

2. Experimental setup and method

A Ti: Sapphire femtosecond laser (800 nm central wavelength, 50 fs pulse duration, 2 kHz repetition rate, maximum energy per pulse of 3 mJ) is used in an optical pump – THz probe configuration, as shown in Fig. 1. The initial laser beam is divided into three beams, two beams are used for THz generation and detection, and the third beam is used as an optical pump to induce TPA in the studied sample. THz probe pulses are generated by OR in a first ZnTe crystal with a laser fluence of about $0.7 mJ/cm^2$ and duration of 150 fs (chirp adjusted in order to optimize the THz signal), and detected by electrooptic sampling (EOS) in a second ZnTe crystal [25]. ZnTe crystals utilized for THz generation and detection are holographic-cut. The crystal used for THz generation has a thickness of 500 μm and its <001 > axis forms an angle of about 55° with the pump polarization direction (horizontal). The crystal used for THz detection has a thickness of 1 mm and its <001 > axis is perpendicular to the optical probe polarization direction, which in turn is parallel to the THz electric field direction in the crystal (both horizontal). These conditions optimize the generated and the detected THz signal. A third ZnTe crystal (500 μm thickness) is used as a sample and it is excited by the optical pump with a laser fluence ranging from $0.01 mJ/cm^2$ to $0.25 mJ/cm^2$. Teflon tapes are positioned just behind the first ZnTe crystal and the studied sample, in order to stop the near-IR laser pulses. The THz radiation generated by the femtosecond optical pump in the studied sample is not detected because its repetition rate (2 kHz) is different from the chopping frequency (850 Hz) of the detection system (heterodyne detection with lock-in amplifier), therefore the THz signal variation detected in the presence

Optics EXPRESS

of the optical pump is only due to the absorption by the free carriers generated by the optical pump in the sample. Moreover, we estimate that about 26% of the optical pump pulse energy is absorbed by the sample within the TPA process when $0.25 mJ/cm^2$ pump fluence is used, which gives an energy conversion efficiency of optical pump to TPA process much higher than the conversion efficiency of the optical pump for THz generation (about 10^{-5}) [26].

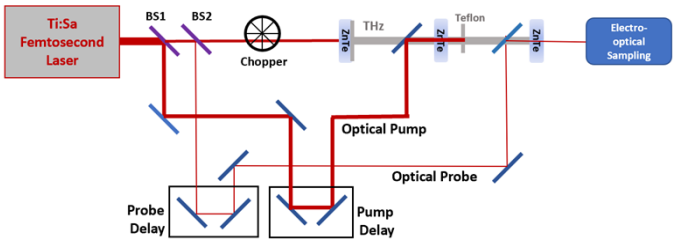

Fig. 1. Optical pump-THz probe setup. The probe delay line is used to reconstruct THz field for a given delay of the optical pump pulse. The pump delay line is used to change the delay between optical pump and the THz probe pulses, probing so the charge transport dynamics induced in the excited sample.

During the experiment the THz probe pulse has a fixed horizontal polarization whereas the optical pump polarization can be changed from parallel to perpendicular, with respect to the THz probe polarization.

We analyze the anisotropy by rotating the sample crystal on a xOy plane by an angle θ measured between the <001 > crystal axis and the y vertical axis (see Fig. 2(b)); with θ_0 we indicate the angle between the optical pump polarization $\hat{e}$ and the y vertical axis. All the experimental results are obtained by measuring the THz transmission of the excited ZnTe as a function of θ for different delays between optical pump and THz probe and different optical pump polarization. All the measurements are done at room temperature.

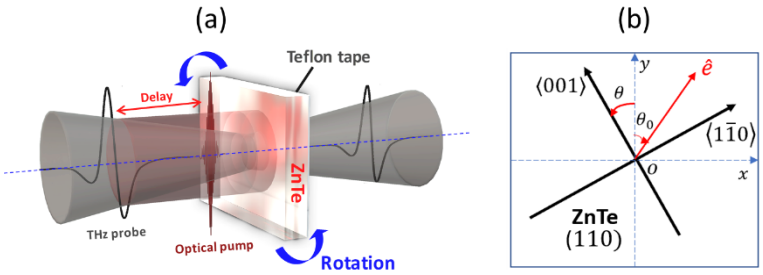

Fig. 2. (a) The schematic of ZnTe sample with orthogonal incident optical pump and THz probe. The optical pump will excite free electrons and then is stopped by a Teflon tape put after the ZnTe sample. (b) The xOy plane is the (110) plane of the holographic-cut ZnTe. Horizontal polarization ($\theta_0 = -90^o$) and vertical polarization ($\theta_0 = 0^o$) of the optical pump are introduced for anisotropy measurements.

3. Theoretical background

ZnTe is a direct bandgap crystal semiconductor, with a bandgap of about 2.3 *eV*. Given the photon energy at 800 *nm*, corresponding to 1.55 *eV*, free electrons in the conduction band and an equivalent population of holes in the valence band can be generated only by TPA. The generated free carriers will efficiently absorb THz probe field by free carrier Inverse Bremsstrahlung absorption process. The relaxation process then may include various paths of decay with recombination rates

Optics EXPRESS

proportional respectively to the electron density (direct band-to-band transition), the square (direct e-h trapping) and the cube (Auger process) of the electron density [27–29]. In semiconductors, relaxation processes via e-h trapping and Auger scattering are expected, but they are effective only at lower band-gap and carrier densities above $10^{18} cm^{-3}$[30]. In our case we expect carrier densities as low as $10^{13} - 10^{14} cm^{-3}$ and therefore e-h trapping and Auger recombination have not significant influence. Furthermore, bulk exciton states in ZnTe have binding energies lying below the thermal agitation energy at room temperature ($k_B T \approx 26\ meV$), therefore in our experimental conditions bound exciton states have very low probability of appearance [31]. For all these reasons we will assume that the laser TPA generated free carrier density has an exponential decay behavior.

The atomic density of ZnTe, $N_{at} = 2 \times 10^{22}\ cm^{-3}$, being much larger than the expected excited electron density (around $10^{14}\ cm^{-3}$), the peak electron density can be estimated using the multi-photon absorption rate equation as $N_0 \approx \sigma_0^{(2)} I_0^2 N_{at} \tau$, where $\sigma_0^{(2)}$ is TPA cross-section, which can be deduced by TPA coefficient β using the relation $\sigma_0^{(2)} = \beta / 2 N_{at} h \nu_0$, where h is Planck constant and ν_0 is the laser pulse central frequency. I_0 is the peak intensity, and $\tau = 150\ fs$ is the optical pluse duration.

The THz intensity transmission by a free electron slab of thickness l can be described by a simple Beer-Lambert law as:

$$T(t) = e^{-\alpha_{fc}(t) l} \tag{1}$$

The characteristic absorption length within TPA is estimated as $1/\beta I_0 \approx 2000\ \mu m$, which is 4 times larger than the sample thickness. Because of the latter consideration and because the pump laser pulse is not focused in the sample, the value of l in Eq. (1) is not the confocal length of the focused beam nor the characteristic TPA absorption length but the sample thickness, $l = 500\ \mu m$. Here we indicate as $\alpha_{fc}(t)$ the free carrier absorption coefficient, which can be written as:

$$\alpha_{fc}(t) = 2 \frac{\Omega}{c} n_I(t) \tag{2}$$

Ω being the THz frequency and $n_I(t)$ being the transient imaginary part of the index corresponding to free carrier relaxation, which depends on the carrier density (t) by the following expression (imaginary part of the square-root of the dielectric function):

$$n_I(t) = \Im \left(\sqrt{1 - i \frac{e^2}{m_e^* \varepsilon_0} \frac{\tau_c}{\Omega (1 - i \Omega \tau_c)} N(t)} \right) \tag{3}$$

where τ_c and m_e^* are the collision time and the electron effective mass, and e and ε_0 the electron charge and the free space permittivity, respectively. The expression (3) represents the variation of the imaginary part of the complex index of an electron plasma when the Drude model is considered to describe it, and cannot be approximated in our experimental conditions because the collision frequency (the inverse of the collision time) could be, in principle, comparable to the plasma frequency, $\omega_{pe} = \sqrt{e^2 N_0 / m_e^* \varepsilon_0}$, and the THz frequency.

4. Experimental results

4.1. THz transmission dynamics

The THz transmission quantity utilized in this work is defined as follows: we calculate the integral of the modulus squared of the THz signal detected by EOS in presence and in absence (the reference) of optical pump (free carriers) respectively and then we take the ratio. The time window for the signal integration is 4 ps, which corresponds to the time window allowing the complete oscillation of the THz electric field, as can be seen in Fig. 3(a), which shows the THz

Optics EXPRESS

signal as measured by EOS before (dark solid line) and just few *ps* after (red solid line) optical pump excitation. The retrieved spectral amplitude is also shown in Fig. 3(b), giving a clear idea of the measured bandwidth. By changing the delay between optical pump and THz probe pulses we experimentally obtain the THz transmission dynamics which is shown as dark solid line in the graph of Fig. 3(c), in the case of excitation by a $0.125 mJ/cm^2$ pump pulse. We can clearly see that two distinct lifetimes have to be considered in order to fit the experimental result. The theoretical curve in Fig. 3(c) (red solid line) is obtained by calculating the THz transmission through a free carrier plasma slab by taking into consideration the simple Drude model described in the section 3, where the density of the plasma slab is described as a bi-exponential decay with two characteristic lifetimes, a fast one of about 50 *ps* and a slow one of about 1.5 *ns*. The short relaxation time seems consistent with the value reported in [32] in similar experimental conditions with respect to our work, while the long relaxation time seems consistent with typical free carrier relaxation times reported in crystal semi-conductors [21]. To reproduce the experimental result some parameters have been fixed by considering the experimental conditions (laser pulse intensity and associated peak electron density: $N_0 \approx 6 \cdot 10^{13}\ cm^{-3}$ at a fluence of $0.1 mJ/cm^2$ and 150 *fs* pulse duration), while the value of $\beta = 5\ cm/GW$ has been taken from [33]. The collision time and the electron effective mass have been retrieved by the simulation, giving respectively the values $\tau_c = 1\ ps$ and m_e^*=$0.12 m_e$. The value of the retrieved collision time is consistent with low intensity exposures and low-density electron-hole plasmas, while the retrieved electron effective mass value is consistent with values previously reported in the literature for ZnTe at room temperature [34]. The percentage of the fast and slow exponential relaxation is around 80% and 20% respectively, indicating that the fast-exponential decay is the dominant process.

4.2. THz free carrier absorption oscillations vs crystal orientation

The THz transmission signal with $0.25 mJ/cm^2$ pump and without pump, for a fixed pump-probe delay and a THz probe polarization set to horizontal, is measured as a function of the crystal orientation, as described in section 2. In Fig. 3(d), the dark curve is the THz transmission of the holographic-cut ZnTe crystal without pump excitation, while the red curve represents the THz transmission obtained when the optical pump is applied just before the probe arrives (a few picoseconds, therefore close to the peak absorption). We can clearly see how a modulation of the THz transmission as a function of the crystal orientation appears when the optical pump is present. This oscillation is attributed to the dependence of the TPA cross-section coefficient with the crystal orientation and laser pulse polarization [17]. The THz transmission oscillation is then due to the oscillation of the initial charge density induced by TPA anisotropy, which induces oscillations of the free carrier absorption coefficient, as a function of the ZnTe <001> axis angle.

For better understanding, both the transmission of the optical pump and the THz transmission by free carriers in presence of the optical pump, are reported in Fig. 4(a) and 4(b), respectively for horizontal and vertical pump polarizations. As can be remarked, the transmission of the sample for the optical pump depends on the crystal orientation (dark squares and solid line). To compare the response of the sample for optical pump and THz probe, we fix the pump delay around the maximal absorption and set the polarization of the optical pump to horizontal ($\theta_0 = -90^o$) (Fig. 4(a)) and vertical ($\theta_0 = 0^o$) (Fig. 4(b)), using a pump fluence of $0.125 mJ/cm^2$. As can be seen, the THz probe transmission oscillation follows the oscillation of the optical pump transmission. This behavior is well explained within the assumed theoretical scenario: the higher the optical pump transmission, the lower the generated free carrier density in ZnTe by TPA, and therefore the lower the THz absorption (or higher the THz transmission) in the free carriers plasma. From Eq. (29) of Ref. [17] it can be deduced that the TPA cross-section $\sigma^{(2)}$ in a holographic-cut semi-insulating cubic crystal has an angle dependence with the <001> axis orientation given by:

$$\sigma^{(2)}(\theta) = \sigma_0^{(2)}\{1 + B[1 + 3cos^2(\theta - \theta_0)]sin^2(\theta - \theta_0)\} \tag{4}$$

Optics EXPRESS

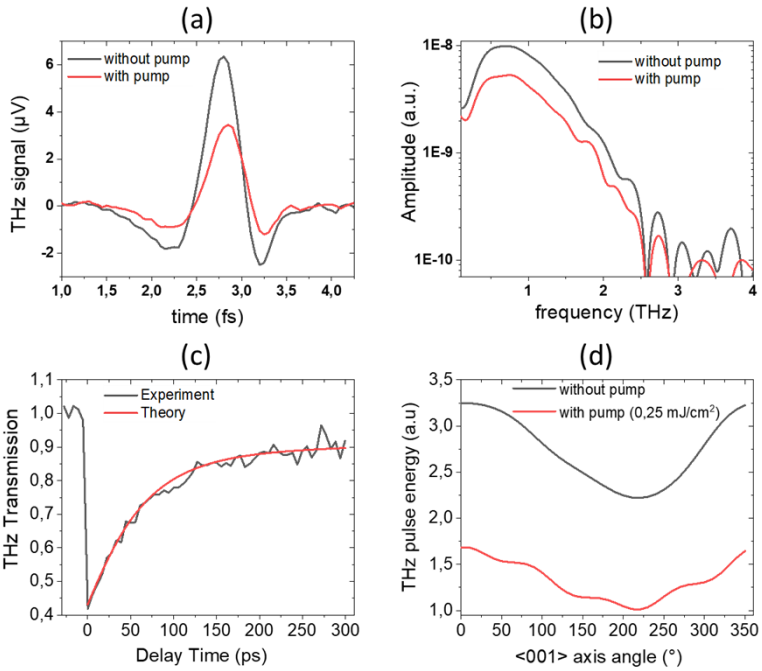

Fig. 3. (a) THz signal measured by EOS before (dark solid line) and few *ps* after optical pump excitation of the studied sample. (b) Retrieved spectral amplitudes after Fourier Transform of the signals in (a). (d) Experimental data (dark line) and the theoretical simulation (red line) of THz transmission by TPA generated free carriers as a function of the optical pump – THz probe delay, within a temporal window of 300 *ps* (pump fluence $0.125 mJ/cm^2$ and 150 *fs* pulse duration). Two exponential recombination times are clearly observable. (c) THz transmission with and without pump excitation as a function of the crystal orientation (pump fluence $0.25 mJ/cm^2$ and 150 *fs* pulse duration).

where θ_0 indicates the pump polarization angle with respect to the vertical axis y, as described in section 2 (Fig. 2(b)). B is an a-dimensional parameter, which is related to the elements of the χ^3 tensor involved in the TPA process. In Fig. 4(c) and (d), we use this model to fit the experimental data, with fixed θ_0 (pump polarization). By adjusting the theoretical and the experimental results we find a value of $B = 0.23$, which is consistent with the value reported in Ref. [17] for a CdTe crystal. As can be seen in Fig. 4(c) and (d), the result is consistent with the TPA anisotropy model, for both pump polarizations, horizontal and vertical, in term of prediction of the position of the hills and the valleys and the shape of the oscillation. The discrepancy between experiment and theory, in the graphs of Fig. 4(c) and 4(d), is attributed to the THz transmission fluctuation with the crystal orientation, which is present even in absence of the optical pump, although this oscillation is randomly distributed and it has not the same structure as the oscillation in presence of the optical pump. The level of this noise can be estimated by observing the Fig. 5(a) for negative delay (before the pump arrives).

4.3. THz free carrier absorption oscillation vs crystal orientation and pump-probe delay

THz transmission amplitude vs angle at different pump delays has been measured. In this case we fix a horizontal pump polarization with a fluence of $0.14 mJ/cm^2$. The THz transmission as a function of the <001 > crystal axis orientation has the same oscillation trend than at zero delay but different oscillation amplitudes, as shown in Fig. 5(a). A remarkable feature which can be remarked by observing the graph of Fig. 5(a) is that the maximum THz oscillation

Optics EXPRESS

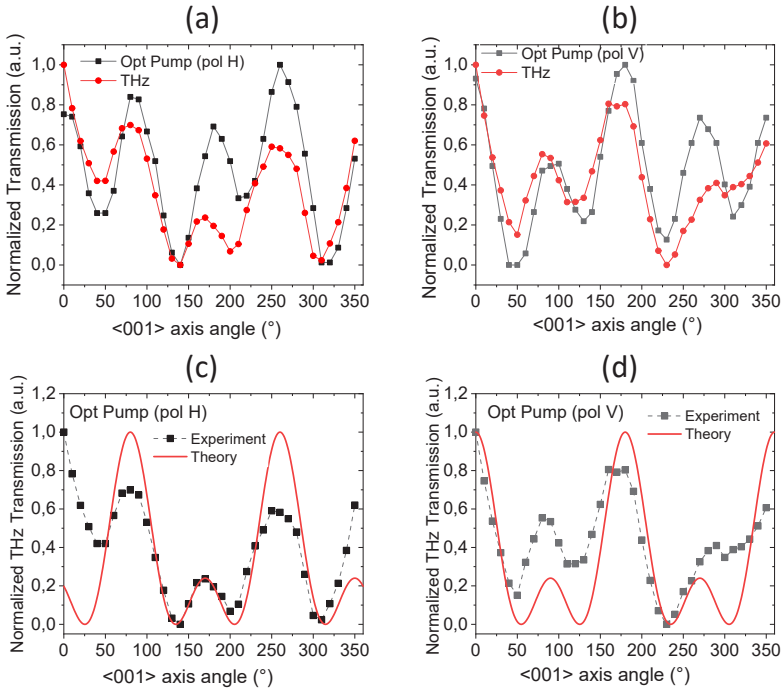

Fig. 4. The output optical pump power oscillates with the <001 > axis angle, and the THz signal follows the pump oscillation, in the case of horizontal (a) and vertical (b) pump polarization. In (c) and (d), we use the model taken from [17] to fit the experimental data for both horizontal and vertical polarizations of the optical pump. All the curves are normalized between 0 and 1.

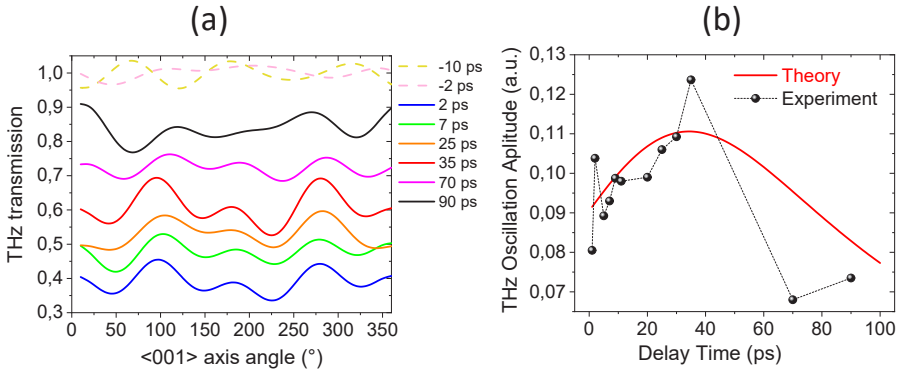

Fig. 5. (a) THz transmission oscillation as a function of the crystal orientation, for several optical pump delay, with polarization set to horizontal, and fluence of $0.14 mJ/cm^2$ (the negative delay time means the pump arrives after the probe, and the observed oscillations are only due to noise). (b) Experimental (black dots and dashed line) and theoretical (red solid line) THz oscillation amplitude as a function of the delay. As can be seen the maximum THz oscillation amplitude appears at a delay of about 35 *ps*. This is well predicted by the theory.

Optics EXPRESS

amplitude is not occurring at zero delay. This behavior is also well predicted by the theory (TPA carrier generation + anisotropic oscillation of the TPA cross-section given by (4) + carrier recombination), and the comparison with the experimental amplitudes is shown in Fig. 5(b). By analyzing the experimental behavior of the THz transmission in the Figs. 5(a), we can observe in fact that the THz transmission oscillation amplitude (ΔT) has a maximum (ΔT_{max}) at a delay of about 35 *ps*.

Remark that this is not a real delayed response of the sample. In fact, the transmission function of the electron plasma, $T(t) = e^{-\alpha_{fc}(t)l}$, is a monotonic function of the time, but when a small modulation of the initial carrier density, ΔN_0, is introduced (because of the anisotropic oscillation of the TPA coefficient with the crystal orientation), the function $\Delta T(t) = |\partial T/\partial N_0| \times \Delta N_0 \propto |\partial \alpha_{fc}(t)/\partial N_0| e^{-\alpha_{fc}(t)l}$ may not be monotonic in time and have a maximum which is delayed with respect to $t = 0$ (excitation time). However, the value of the delay at which this maximum oscillation amplitude arrives (in our case around 35 ps) is very sensitive to the experimental conditions (pump laser intensity) and the physical parameters of the system (peak carrier density, electron effective mass, collision time, lifetimes). This can be experimentally verified by plotting ΔT as a function of the delay, considering the experimental data reported in Fig. 5(a), and the result is illustrated with black dot and dashed line in Fig. 5(b). Within the proposed model, if the value of the maximum THz oscillation amplitude, ΔT_{max}, is essentially determined by the value of the parameter B, here fixed to 0.23, the delayed position at which this maximum is reached depends weakly on the value of the parameter B and strongly on the other important parameters involved in the model and described in the paragraph 4.1, as the electron effective mass, the collision time, and the two characteristic lifetimes. By considering the values of the electron effective mass, the collision time, and the two lifetimes reported in the paragraph 4.1 we were able to theoretically predict a maximum THz oscillation amplitude occurring at around 35 *ps*, and the theoretical curve (red solid line in Fig. 5(b)) is satisfactory in agreement with the experimental result.

We can conclude that the simple theoretical model proposed here is consistent not only with the description of the carrier generation and relaxation dynamics, but equally with the description of the dynamics of the charge anisotropy initiated by TPA.

4.4. THz absorption oscillations vs crystal orientation in surface structured ZnTe with ripples

One of the main objectives of this work is to study if and how a permanent anisotropy, generated by pre-structuring the sample on its surface by using ultrashort laser, influences the transient charge anisotropy induced by TPA. The structures consist in periodic ripples photowritten on the whole surface, having an average period of about 800 - 850 *nm*, on a average depth of about 300 *nm*, forming an angle of about 25–30° with the <001 > axis of the ZnTe sample, as indicated in Fig. 6, where scanning electron microscopy (SEM) and atomic force microscopy (AFM) images of the ripples are shown.

The sample surfaces were textured using a Tangor HP femtosecond laser (Amplitude Systems, France) and a galvanometric scanner (GmbH's intelliSCAN 14, Scanlab, Germany). The laser pulses have central wavelength of 1030 *nm* and pulse duration around 400 *fs*. The laser beam was linearly polarized. All the samples were placed on 3D-XYZ translation stages. The galvanometric scanner was finally associated with a f-theta lens of 100 mm, and surface ripples were generated at a fluence of 2 J/cm^2. The beam spot size was about 33 μm in diameter. For large area ripples formation, the pulse-to-pulse spacing and the offset between scanning lines were kept identic and equal to 5 μm. These structures are photowritten on both the input and the output faces of the sample with the same angle. The periodic structures, generated on both ZnTe surfaces, by using ultrashort laser photo-inscription, have remarkable quality, as can be seen in Fig. 6.

Optics EXPRESS

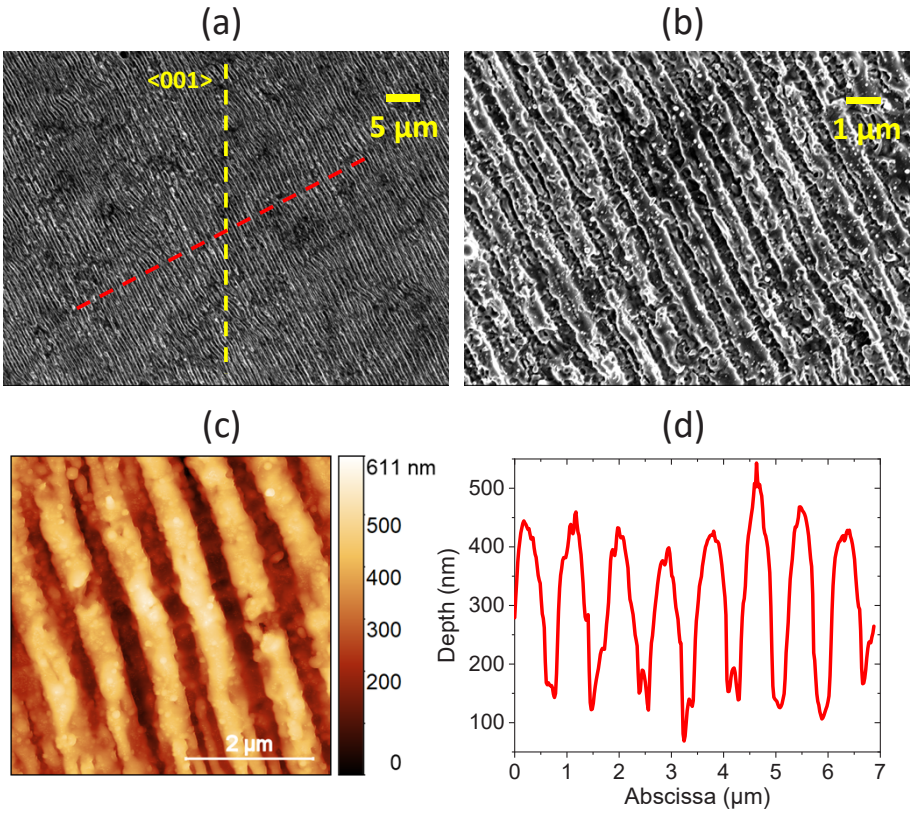

Fig. 6. (a), (b) SEM images of the ripples photowritten on the ZnTe surfaces (two different magnifications are given). The yellow dashed line in Fig. 6(a) is a guide for the eyes and indicates the direction of the <001 > axis of ZnTe, while the red dashed line represents the new optical axis introduced by ripples. (c) AFM image of the surface ripples, with a false color scale indicating the depth level. (d) Surface scanning with the AFM tip along the x axis, giving an average depth variation of about 300 *nm* and a deduced (projection along the direction perpendicular to ripples) average period of about 800 - 850 *nm*.

We first investigate the effect of ripples on the static response of ZnTe by measuring the sample transmission for the optical pump and the THz probe with respect to <001 > axis orientation, by using horizontally polarized optical and THz beams. Surface ripples have big effect on the optical pump transmission, by drastically reducing the transmitted power (about 7 times for a $0.125 mJ/cm^2$ input fluence), but in particular by drastically changing the angular dependence on the <001 > axis orientation. This last characteristic can be observed by comparing the relative transmission (the mean value has been removed) of the optical pump for three different input powers, as a function of the crystal orientation without ripples (and therefore only due to TPA anisotropy) (Fig. 7(a)), and with ripples (Fig. 7(b)). As expected, at a very low input fluence of about $0.01 mJ/cm^2$, the oscillating behavior of the sample transmission disappears, when the anisotropy is due only to TPA (Fig. 7(a)), but on the contrary it keeps in presence of surface ripples. This indicates that in the first case the anisotropy effect is self-induced by the optical pump and it disappears when TPA is no more effective at low fluences, while in the second case the effect is permanent because is due to permanent structures photowritten on the surface. By the contrary, ripples seem having small effect on static THz transmission (no pump excitation). In fact, if the presence of surface ripples reduces the static THz transmission of about 30%,

Optics EXPRESS

probably because of a change in surface reflectivity and transmissivity due to the presence of ripples, it has no significative effect on the angular dependence of the THz signal with crystal orientation, as shown in Fig. 7(c). The strong effect on the angular dependence of the optical pump transmission with <001 > axis orientation can be explained by a relatively strong coupling due to the fact that the values of the optical wavelength and the ripples average period are very close. This also explains why this effect is negligible in the case of static THz transmission (wavelength of 300 μm at 1 THz).

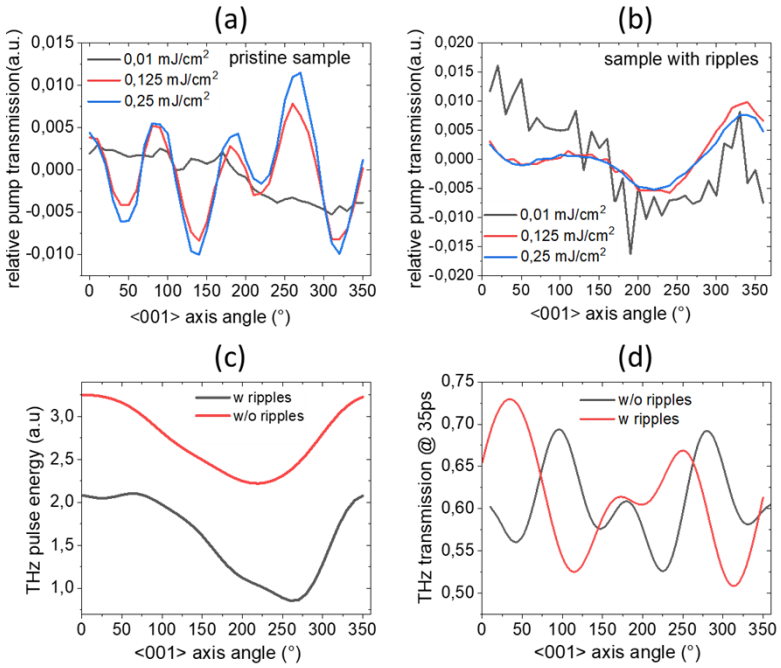

Fig. 7. (a) Relative (the average value has been removed) optical pump transmission vs crystal orientation on a pristine ZnTe, for different input optical pump fluences. (b) Same measurement as in (a) but in presence of surface ripples. (c) THz pulse energy (value proportional to) transmitted by the ZnTe sample as a function of the crystal orientation, with (dark solid line) and without (red solid line) surface ripples. (d) free carrier THz transmission as a function of the crystal orientation for an optical pump-THz probe delay of 35 ps, with pump fluence of $0.25 mJ/cm^2$, and horizontal polarization.

If the angular behavior of the static THz transmission with the <001 > axis orientation is not affected by the presence of surface ripples, this is not the case of the transient THz transmission in presence of free carriers induced by TPA. In this case in fact a significant angular shift (angle dependent) is observed in the THz transmission curve, as shown in Fig. 7(d) for a delay of 35 ps (corresponding to the delay where a maximum oscillation amplitude is observed). We also observe that this shift is not constant but it depends on the angle. This behavior can be explained by assuming a birefringence effect induced by ripples on the surface, which changes the polarization of the optical pump after the input surface. This optical pump polarization change is responsible for the angular shift observed on the THz transmission curve, as expected by considering the TPA anisotropy model described in section 4.

Surprisingly surface pre-structuring with ripples seems affecting also the free carrier relaxation dynamics, by changing the value of the fast characteristic relaxation time. In Fig. 8(a) we show the experimental (dark solid line) and theoretical (red solid line) relaxation decay up to 1 ns in presence of surface ripples for a fixed crystal orientation. To fit this relaxation decay, all

Optics EXPRESS

the parameters are maintained equal with respect to the case without ripples (paragraph 4.1, Fig. 3(c)) excepted the parameter corresponding to the fast relaxation lifetime, which has to be set now at 90 *ps* instead of 50 *ps*. This result is confirmed by measuring the relaxation dynamics of the oscillating THz signal transmitted by free carriers, averaged over 360° crystal orientation, for the pristine sample first, and then for the same sample but pre-structured with ripples. The experimental results (dots and dashed lines) and the corresponding simulations (solid lines) are shown in Fig. 8(b). We can notice that the experimental curve in Fig. 8(a) presents a higher level of noise with respect to the one presented in Fig. 3(c) (no ripples). This noise can be explained by the presence of surface ripples. In fact, the surface birefringence introduced by ripples highlights the phase fluctuations of the optical pump polarization components, resulting in a significative polarization jitter. The noise is due to the fact that the THz transmission is highly sensitive to the pump polarization. However, the increase of the noise can only increase the uncertainty of the measured lifetime and not its average value, therefore this effect cannot be attributed to an artifact due to the high noise level. A possible empirical explanation of this effect is that the fast relaxation process is related to phenomena happening on or close to the ZnTe surfaces. Among the scenarios proposed to explain this effect there is a relatively fast transient change of the surface reflectivity, induced by the optical pump at THz frequencies. This would give the impression of a fast depletion of charge in the volume. However, in this case the Drude frame would be preserved because the consequence of this scenario would be only an overestimation of the initial carrier density. Another possibility is that we observe a relatively fast trapping of electrons by impurities due to structural defects, which are much more numerous close to the interface. This would give a fast and strong depletion of charge close to the interface, which in turn can give a transient change of reflectivity at THz frequencies. In this case changing the interface properties by pre-structuring it, can change the electron dynamics after pump excitation of the crystal semiconductor. In fact, the presence of impurities due to structural defects at the interface of a crystal semiconductor is a common feature. This is why it is important to study how a pre-structuration of the interface can change the anisotropic and electronic properties of a crystal semiconductor. However, a more detailed analysis is needed to validate these hypotheses, and it is matter for future investigations.

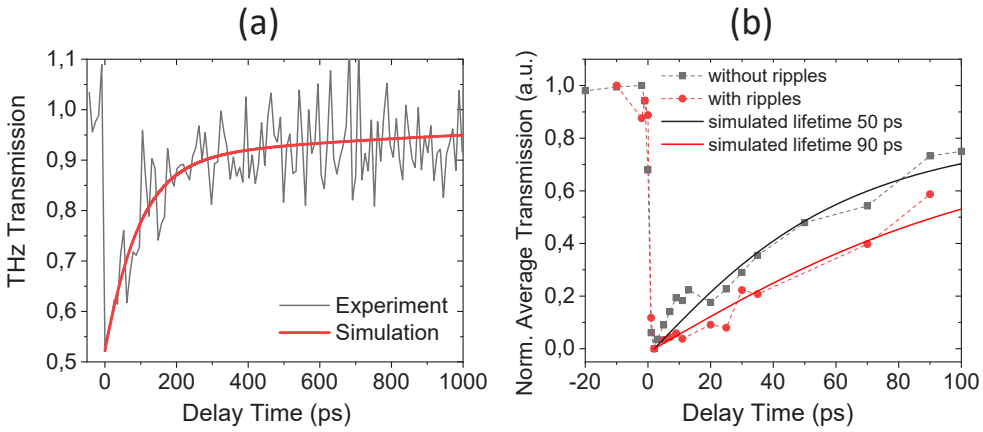

Fig. 8. (a) Experimental and theoretical relaxation dynamics measured and calculated until 1 ns in presence of surface ripples. (b) Normalized THz transmission by free carrier (averaged over 360° crystal orientation) in absence (dark squares and dashed line) and in presence (red circles and dashed line) of surface ripples. The solid lines correspond to theoretical simulations of exponential decays with 50 *ps* (dark solid line) and 90 *ps* (red solid line) lifetimes.

Optics EXPRESS

5. Conclusion

Using THz pulses, we probed the anisotropic relaxation dynamics of TPA generated free carriers in bulk ZnTe with density as low as 6×10^{13} cm^{-3}. Transient anisotropy induced within the TPA process itself, and consisting in an oscillation of the THz signal transmitted by TPA generated free carriers as a function of the crystal orientation, have been analyzed for pristine and surface pre-structured ZnTe, as a function of the delay between optical pump and THz probe. Pre-structuring the surface sample with ripples showed a strong influence on the optical pump (the source of free carriers), introducing at the same time a polarizing function (polarization directional coupling) and a birefringence function (introduction of an optical axis perpendicular to ripples) on the ZnTe surfaces, while it showed low influence on the sample static THz transmission. However, surface ripples have strong influence on the THz signal transmitted by the photo-generated free carriers, and the corresponding anisotropy, because of its sensitivity to the optical pump intensity and polarization state, which are strongly influenced by the introduction of the surface structures. In particular, the birefringence introduced by the ripples on the input surface changes the polarization of the optical pump, resulting in an angle dependent phase shift of the oscillating free carrier THz transmission. The relaxation dynamics shows clearly two distinct lifetimes, a long one of about 1.5 *ns*, and a short one of about 50 *ps* in absence of ripples, which becomes equal to about 90 *ps* in presence of ripples. The fact that only the fast decay is significantly influenced by ripples could indicate that this lifetime is related to a process happening at the interface or close to it, as for example a transient surface reflectivity change at THz frequencies, induced by the optical pump. A simple model based on classic Drude theory of free carrier absorption, as well as the anisotropy description in term of dependence of the TPA coefficient on the crystal orientation and on the laser pulse polarization, has been adopted and showed a satisfactory consistence with the observed experimental results. This type of analysis is applied here for surface pre-structured ZnTe semi-insulating crystal, but it could be applied in principle for any material. Analyzing the influence of laser structuring on transport properties can have an important impact for future applications in the domains of ultrafast laser-processed functional engineered surfaces and materials.

Acknowledgments. This work was supported by the LABEX MANUTECH-SISE (ANR-10-LABX-0075) of Université de Lyon, within the "Plan France 2030" operated by the French National Research Agency (ANR), and the program "Investissements d'Avenir" (ANR-11-IDEX-0007). Authors equally acknowledge the GIE Manutech-USD platform for allowing the realization of the surface ripples on the ZnTe sample.

Disclosures. The authors declare no conflicts of interest.

Data availability. Data underlying the results presented in this paper are not publicly available at this time but may be obtained from the authors upon reasonable request.

References

1. M. Malinauskas, A. Žukauskas, S. Hasegawa, Y. Hayasaki, V. Mizeikis, R. Buividas, and S. Juodkazis, "Ultrafast laser processing of materials: from science to industry," Light: Sci. Appl. **5**(8), e16133 (2016).
2. S. Papa, A. A. Khalil, H. Hamzeh-Cognasse, M. Thomas, M. Maalouf, Y. Di Maio, X. Sedao, A. Guignandon, and V. Dumas, "Dual-functionalized titanium by ultrafast laser texturing to enhance human gingival fibroblasts adhesion and minimize Porphyromonas gingivalis colonization," Appl. Surf. Sci. **606**, 154784 (2022).
3. A. Nakhoul, A. Rudenko, X. Sedao, N. Peillon, J. P. Colombier, C. Maurice, and G. Kermouche, "Energy feedthrough and microstructure evolution during direct laser peening of aluminum in femtosecond and picosecond regimes," J. Appl. Phys. **130**(1), 015104 (2021).
4. H. D. Nguyen, X. Sedao, C. Mauclair, G. Bidron, N. Faure, E. Moreno, and S. Razvan, "Non-diffractive Bessel beams for ultrafast laser scanning platform and proof-of-concept side-wall polishing of additively manufactured parts," Micromachines **11**(11), 974 (2020).
5. J. Bonse, S. V. Kirner, and J. Krüger, "Laser-induced periodic surface structures (LIPSS)," Handbook of laser micro-and nano-engineering 1–59 (2020).
6. J. Bonse, "Quo vadis LIPSS? - recent and future trends on laser-induced periodic surface structures," Nanomaterials **10**(10), 1950 (2020).

Optics EXPRESS

7. J. P. Colombier, A. Rudenko, E. Silaeva, H. Zhang, X. Sedao, E. Bévillon, and S. Razvan, "Mixing periodic topographies and structural patterns on silicon surfaces mediated by ultrafast photoexcited charge carriers," Phys. Rev. Res. **2**(4), 043080 (2020).
8. E. W. Van Stryland, H Vanherzeele, M. A. Woodall, M. J. Soileau, A. L. Smirl, S. Guha, and T. F. Boggess, "Two photon absorption, nonlinear refraction, and optical limiting in semiconductors," Opt. Eng. **24**(4), 613–623 (1985).
9. J. H. Bechtel and W. L. Smith, "Two-photon absorption in semiconductors with picosecond laser pulses," Phys. Rev. B **13**(8), 3515–3522 (1976).
10. E. W. Van Stryland, M. A. Woodall, H. Vanherzeele, and M. J. Soileau, "Energy band-gap dependence of two-photon absorption," Opt. Lett. **10**(10), 490–492 (1985).
11. P. Liu, W. L. Smith, H. Lotem, J. H. Bechtel, N. Bloembergen, and R. S. Adhav, "Absolute two-photon absorption coefficients at 355 and 266 nm," Phys. Rev. B **17**(12), 4620–4632 (1978).
12. J. I. Dadap, G. B. Focht, D. H. Reitze, and M. C. Downer, "Two-photon absorption in diamond and its application to ultraviolet femtosecond pulse-width measurement," Opt. Lett. **16**(7), 499–501 (1991).
13. T. F. Boggess, O. W. Jeffrey, and G. C. Valley, "Two-photon absorption and anisotropic transient energy transfer in BaTiO 3 with 1-psec excitation," J. Opt. Soc. Am. B **7**(12), 2255–2258 (1990).
14. K. W. DeLong, K. B. Rochford, and G. I. Stegeman, "Effect of two-photon absorption on all-optical guided-wave devices," Appl. Phys. Lett. **55**(18), 1823–1825 (1989).
15. V. Mizrahi, K. W. DeLong, G. I. Stegeman, M. A. Saifi, and M. J. Andrejco, "Two-photon absorption as a limitation to all-optical switching," Opt. Lett. **14**(20), 1140–1142 (1989).
16. K. W. DeLong and G. I. Stegeman, "Two-photon absorption as a limitation to all-optical waveguide switching in semiconductors," Appl. Phys. Lett. **57**(20), 2063–2064 (1990).
17. M. D. Dvorak, W. A. Schroeder, D. R. Andersen, A. L. Smirl, and B. S. Wherrett, "Measurement of the anisotropy of two-photon absorption coefficients in zincblende semiconductors," IEEE J. Quantum Electron. **30**(2), 256–268 (1994).
18. D. C. Hutchings and B. S. Wherrett, "Theory of anisotropy of two-photon absorption in zinc-blende semiconductors," Phys. Rev. B **49**(4), 2418–2426 (1994).
19. D. C. Hutchings and B. S. Wherrett, "Theory of the polarization dependence of two-photon absorption in zinc-blende semiconductors," J. Mod. Opt. **41**(6), 1141–1149 (1994).
20. F. Sanjuan, G. Gaborit, and J. L. Coutaz, "Influence of two-photon absorption anisotropy on terahertz emission through optical rectification in zinc-blende crystals," J. Infrared, Millimeter, Terahertz Waves **39**(4), 378–386 (2018).
21. A. Kanevce, D. Kuciauskas, D. H. Levi, A. M. Allende Motz, and S. W. Johnston, "Two dimensional numerical simulations of carrier dynamics during time-resolved photoluminescence decays in two-photon microscopy measurements in semiconductors," J. Appl. Phys. **118**(4), 045709 (2015).
22. A. Opanowicz, K. Marinova, H. Liebing, and W. Ruppel, "Luminescence of highly excited ZnTe crystals," Phys. Status Solidi B **75**(2), 471–481 (1976).
23. J. B. Baxter and C. A. Schmuttenmaer, "Carrier dynamics in bulk ZnO. II. Transient photoconductivity measured by time-resolved terahertz spectroscopy," Phys. Rev. B **80**(23), 235206 (2009).
24. G. Vampa, T. J. Hammond, N. Thiré, B. E. Schmidt, F. Légaré, C. R. McDonald, T. Brabec, D. D. Klug, and P. B. Corkum, "All-Optical Reconstruction of Crystal Band Structure," Phys. Rev. Lett. **115**(19), 193603 (2015).
25. K. Reimann, "Table-top sources of ultrashort THz pulses," Rep. Prog. Phys. **70**(10), 1597–1632 (2007).
26. S. Vidal, J. Degert, M. Tondusson, E. Freysz, and J. Oberlé, "Optimized terahertz generation via optical rectification in ZnTe crystals," J. Opt. Soc. Am. B **31**(1), 149–153 (2014).
27. R. W. Boyd, "*Nonlinear optics*," Academic press (2020).
28. R. N. Hall, "Recombination processes in semiconductors," Proceedings of the IEE-Part B: Electronic and Communication Engineering **106**, 923–931 (1959).
29. Y. C. Shen, G. O. Mueller, S. Watanabe, N. F. Gardner, A. Munkholm, and M. R. Krames, "Auger recombination in InGaN measured by photoluminescence," Appl. Phys. Lett. **91**(14), 141101 (2007).
30. R. Aleksiejūnas, Z. Podlipskas, S. Nargelas, A. Kadys, M. Kolenda, K. Nomeika, and G. Tamulaitis, "Direct Auger recombination and density-dependent hole diffusion in InN," Sci. Rep. **8**(1), 4621 (2018).
31. E. Hendry, M. Koeberg, and M. Bonn, "Exciton and electron-hole plasma formation dynamics in ZnO," Phys. Rev. B **76**(4), 045214 (2007). doi:10.1103/PhysRevB.76.045214
32. Hu Deng, Linyu Chen, Weiwei Qu, Quancheng Liu, Samuel Danso, and Liping Shang, "Photoinduced carrier dynamics in bulk ZnTe using optical-pump terahertz-probe spectroscopy," Opt. Eng. **59**(05), 1 (2020). doi:10.1117/1.OE.59.5.056101
33. A. A. Said, M. Sheik-Bahae, D. J. Hagan, T. H. Wei, J. Wang, J. Young, and E. W. Van Stryland, "Determination of bound-electronic and free-carrier nonlinearities in ZnSe, GaAs, CdTe, and ZnTe," J. Opt. Soc. Am. B **9**(3), 405–414 (1992).
34. S. Shokhovets, O. Ambacher, and G. Gobsch, "Conduction-band dispersion relation and electron effective mass in III-V and II-VI zinc-blende semiconductors," Phys. Rev. B **76**(12), 125203 (2007).